Preprint typeset in JHEP style - HYPER VERSION

The spatial string tension in the deconfined phase of three dimensional QCD in the large N limit

J. Kiskis

Department of Physics, University of California, Davis, CA 95616.
E-mail: jekiskis@ucdavis.edu

R. Narayanan

Department of Physics, Florida International University, Miami, FL 33199.
E-mail: rajamani.narayanan@fiu.edu

Abstract: We numerically compute the spatial string tension in the deconfined phase of three dimensional QCD in the large N limit. Our results clearly show that the string tension grows linearly with temperature.

Keywords: Large N QCD, Deconfined phase, Spatial string tension.

Three dimensional QCD on a symmetric torus is considered in the large N limit. This theory is known to be in the deconfined phase for $T_1 < T < T_2$ [1]. T_1 is the temperature at which one of the three Z_N symmetries is broken and T_2 is the temperature at which two of the three Z_N symmetries are broken[1].

At leading order in $1/N$, the string tension is independent of the temperature in the confined phase ($T < T_1$), and it was computed using reduction [2]. Since the Z_N symmetry is broken only in one direction in the deconfined phase, spatial Wilson loops in the plane perpendicular to the broken direction are expected to show confining behavior. This has been numerically observed in the deconfined phase of SU(2) Yang-Mills theory in four dimensions [3].

We use the standard Wilson gauge action,

$$S = bN \sum_{\mathbf{n},\hat{\mathbf{i}}\neq\hat{\mathbf{j}}} \text{Re Tr} U_i(\mathbf{n}) U_j(\mathbf{n}+\hat{\mathbf{i}}) U_i^\dagger(\mathbf{n}+\hat{\mathbf{j}}) U_j^\dagger(\mathbf{n}), \tag{1}$$

on a L^3 lattice with periodic boundary conditions. The 't Hooft limit is obtained by keeping the coupling $b = \frac{1}{g^2 N}$ fixed as we take $N \to \infty$. We use the tadpole improved lattice coupling [4],

$$b_I = be(b) = \frac{1}{6NL^3}\langle S \rangle, \tag{2}$$

instead of the lattice coupling b. We approach the continuum limit in the deconfined phase by taking $b_I \to \infty$ and $L \to \infty$ keeping the physical temperature, $T = \frac{b_I}{L}$ fixed. The upper and lower limits of the deconfined phase have been numerical estimated [1] to be

$$\begin{aligned} T_1 &= \lim_{L\to\infty} \tfrac{b_{I1}(L)}{L} = 0.160(13) \\ T_2 &= \lim_{L\to\infty} \tfrac{b_{I2}(L)}{L} = 0.263(19). \end{aligned} \tag{3}$$

We used $L = 4, 5, 6, 7$ and $N = 59$ to extract the behavior of the string tension as a function of the temperature in the deconfined phase. We also used $L = 4$ and $N = 47$ to verify that $N = 59$ was large enough for us to ignore finite N effects. The complete list of couplings used in the numerical analysis can be found in Table 1, and the full range from T_1 and T_2 has been covered. A plot of the average energy $e(b)$ listed in Table 1 is plotted in Figure 1 along with a fit that includes a $\frac{1}{b}$ and a $\frac{1}{b^2}$ term. The tadpole improved coupling removes some large lattice spacing effects that are common to all observables.

We used an order parameter based on the Polyakov loop and defined by [5]

$$\begin{aligned} \bar{P}_i &= \langle P_i \rangle \\ P_i &= \frac{1}{2L^2} \sum_{\mathbf{n}} (1 - \left| \frac{1}{N} Tr \mathcal{P}_i(\mathbf{n}) \right|^2) \\ \mathcal{P}_i(\mathbf{n}) &= \prod_{m=1}^{L} U_i(\mathbf{n} + m\hat{\mathbf{i}}), \end{aligned} \tag{4}$$

[1] T_2 can be taken to infinity by working on an asymmetric torus with one short (temperature) direction and two long (spatial) directions.

to ensure that we are in the deconfined phase. The quantity P_i takes values in the range $[0, 0.5]$ on any gauge field background, and we choose the directions $i = 1, 2, 3$ such that such that $P_1 < P_2 < P_3$. The deconfined phase corresponds to $\bar{P}_1 < 0.5$ and $\bar{P}_2 = \bar{P}_3 = 0.5$ within errors. The data presented in Table 1 and plotted in Figure 2 shows this to be the case.

We use computational techniques identical to the ones described in [2] to compute the static potential in the deconfined phase of large N QCD for spatial Wilson loops. As discussed in [2], our links in the $1-2$ plane are smeared while the links in direction 3 are not smeared. We have set the smearing factor to $f = 0.1$ and the number of smearing steps to $n = 25$. We compute the expectation values of all $L_2 \times L_3$ loops, $W(L_2, L_3)$, in the $2-3$ (spatial) plane with $1 \leq L_2, L_3 \leq 10$. Keeping L_2 fixed, we fit

$$\ln W(L_2, L_3) = -A - V(L_2)L_3. \tag{5}$$

Since $W(L_2, L_3)$ becomes small as $L_2 L_3$ becomes big, we do not use all values of L_3 for the fit. The range of L_3 is determined such that the relative error of the fit per degree of freedom (number of values of L_3 used in the fit) is less than 0.1%, and this typically included all loops with $1 \leq L_2 L_3 \leq 40$. The static potential $V(L_2)$ is subsequently fit to

$$V(L_2) = C_0 + \frac{C_1}{L_2} + \Sigma L_2. \tag{6}$$

The results for C_0, C_1 and $\sqrt{\Sigma}$ are shown in Table 1. The performance of the fits for $L = 4, 5, 6, 7$ at $N = 59$ can be seen in the plots of the static potential in Figure 3. A comparison of the values of $\sqrt{\Sigma}$ for $N = 47$ and $N = 59$ at $L = 4$ for the three different values of b shows that finite N effects are small at $N = 59$.

The last column in Table 1 provides all the results obtained in this paper for the spatial string tension at several values of the temperature in the deconfined phase. If we use high temperature dimensional reduction similar to the arguments in [3], the effective two dimensional coupling is

$$b_2 = bL. \tag{7}$$

If the spatial string tension in the deconfined phase is equal to the string tension in the two dimensional theory, then we expect [6]

$$\Sigma = \frac{1}{4b_2} = \frac{1}{4bL}. \tag{8}$$

A plot of Σ versus $\frac{1}{bL}$ is shown in Figure 4. The combined data at the four different values of L are fit to a straight line. Considering that the value of T is modest and that its value is not large, the fit is surprisingly consistent with the prediction in (8).

Another way to plot Figure 4 is to convert the axes to physical units (physical string tension vs. physical temperature) and use tadpole improved coupling. Such a plot is shown in Figure 5. At the same physical T, larger L corresponds to finer lattice spacing. Thus finite spacing effects appear as the scatter in L in this plot, and the fit coefficients are slightly different from those in Figure 4.

If we assume (8) to be valid in the entire region of the deconfined phase and use $\frac{1}{8\pi b^2}$ [7] for the string tension in the confined phase, continuity of the string tension across the phase transition suggests that $T_1 = \frac{1}{2\pi}$ consistent with (3).

Alternatively, we can compare the $L = 5$ results here and in [2]. When the measured values for $\sqrt{\Sigma}$ at $T = 0$ are extrapolated to $b = 1.00$ we obtain 0.232(11), which compares favorably with the corresponding value in Table 1.

If the spatial string tension is indeed continuous at T_1, then we have a picture for the $N = \infty$ limit in which the spatial and temporal string tensions are equal and independent of T for $T < T_1$. At T_1, the temporal string tension falls to zero discontinuously, and the spatial string tension begins to grow linearly with T.

Acknowledgments

R.N. acknowledges partial support by the NSF under grant number PHY-055375.

References

[1] R. Narayanan, H. Neuberger and F. Reynoso, Phys. Lett. B **651**, 246 (2007) [arXiv:0704.2591 [hep-lat]].

[2] J. Kiskis and R. Narayanan, JHEP **0809**, 080 (2008) [arXiv:0807.1315 [hep-th]].

[3] G. S. Bali, J. Fingberg, U. M. Heller, F. Karsch and K. Schilling, Phys. Rev. Lett. **71**, 3059 (1993) [arXiv:hep-lat/9306024].

[4] G. P. Lepage, arXiv:hep-lat/9607076.

[5] G. Bhanot, U. M. Heller and H. Neuberger, Phys. Lett. B **113**, 47 (1982).

[6] D. J. Gross and E. Witten, Phys. Rev. D **21**, 446 (1980).

[7] D. Karabali, C. j. Kim and V. P. Nair, Phys. Lett. B **434**, 103 (1998) [arXiv:hep-th/9804132].

L	N	b	e	$\langle P_1 \rangle$	$\langle P_2 \rangle$	$\langle P_3 \rangle$	C_0	C_1	$\sqrt{\Sigma}$
4	47	0.900	0.801529(17)	0.45386(22)	0.49813(4)	0.49927(2)	−0.0532(15)	0.1586(16)	0.28283(49)
4	47	1.000	0.823036(15)	0.42530(21)	0.49771(6)	0.49922(2)	−0.0420(13)	0.1344(13)	0.26521(40)
4	47	1.100	0.840264(14)	0.40359(25)	0.49479(14)	0.49823(5)	−0.0306(10)	0.1131(11)	0.25051(36)
4	59	0.900	0.801499(14)	0.45513(32)	0.49750(11)	0.49896(5)	−0.05167(15)	0.1569(15)	0.28327(42)
4	59	1.000	0.823003(13)	0.42379(15)	0.49861(3)	0.49947(1)	−0.0595(16)	0.1520(18)	0.26114(63)
4	59	1.100	0.840220(11)	0.40016(17)	0.49744(6)	0.49922(2)	−0.0455(12)	0.1274(13)	0.24827(52)
5	59	1.000	0.822623(9)	0.49381(12)	0.49776(4)	0.49907(2)	−0.05458(53)	0.15586(59)	0.24446(21)
5	59	1.125	0.843795(8)	0.45277(22)	0.49831(6)	0.49928(3)	−0.05148(56)	0.13954(57)	0.22553(22)
5	59	1.250	0.860343(7)	0.42594(15)	0.49865(3)	0.49955(1)	−0.04660(43)	0.12423(46)	0.21094(21)
5	59	1.375	0.873694(6)	0.40449(16)	0.49764(5)	0.49915(2)	−0.03857(37)	0.10847(40)	0.19909(19)
6	59	1.200	0.854075(5)	0.48168(19)	0.49848(4)	0.49947(1)	−0.05681(30)	0.14171(32)	0.20503(13)
6	59	1.350	0.871170(5)	0.45220(14)	0.49875(2)	0.49952(1)	−0.04668(23)	0.12105(25)	0.19082(12)
6	59	1.500	0.884638(4)	0.42848(15)	0.49852(3)	0.49935(2)	−0.04140(19)	0.10774(21)	0.17810(12)
6	59	1.650	0.895545(4)	0.40783(14)	0.49800(3)	0.49922(2)	−0.03671(17)	0.09652(19)	0.16788(11)
7	59	1.325	0.868531(4)	0.49794(4)	0.49889(2)	0.49950(1)	−0.04721(15)	0.12403(17)	0.19006(8)
7	59	1.400	0.875947(3)	0.48714(17)	0.49713(5)	0.49907(2)	−0.04274(15)	0.11540(16)	0.18275(8)
7	59	1.575	0.890335(3)	0.45255(11)	0.49864(3)	0.49951(1)	−0.03855(12)	0.10265(14)	0.16857(7)
7	59	1.750	0.901710(3)	0.43089(13)	0.49850(3)	0.49947(1)	−0.03740(10)	0.09472(11)	0.15605(7)

Table 1: The various parameters (L, N and b), the average value of the plaquette, e, Polyakov loop order parameter in the three directions and the three parameters in the fit of the static potential. Each set has 800 measurements. All errors are obtained using single elimination jackknife.

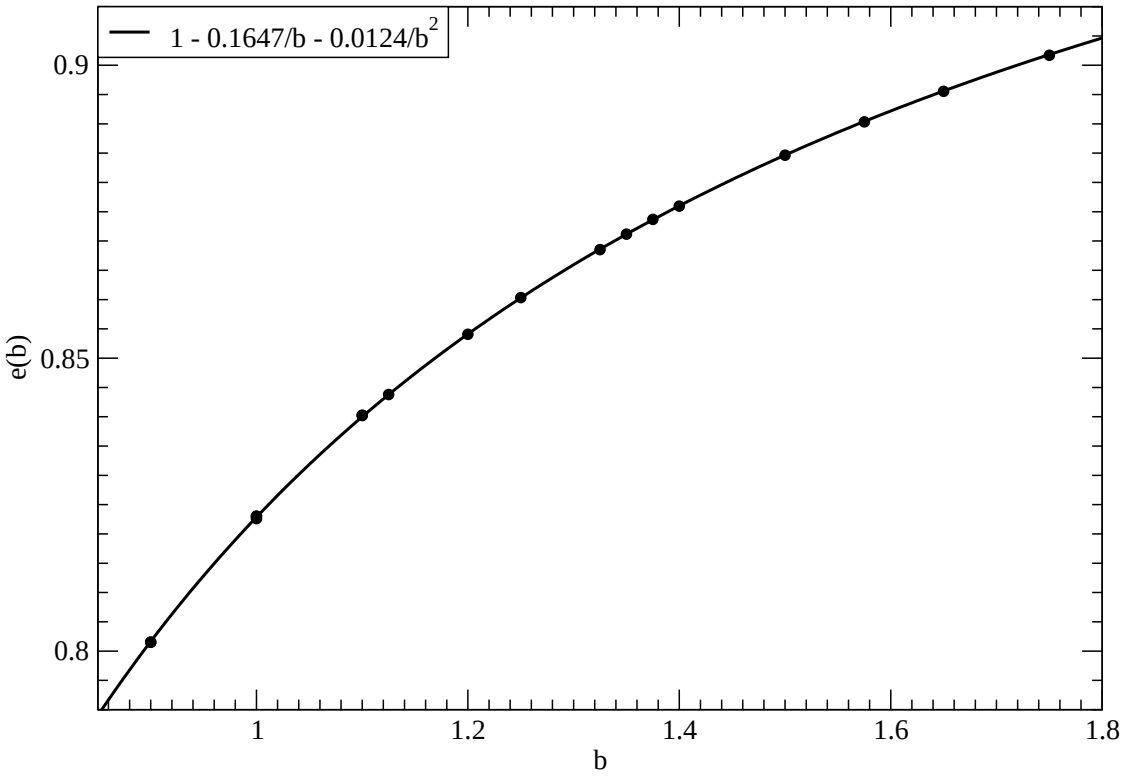

Figure 1: Plot of $e(b)$ as a function of b for all the data sets in Table 1.

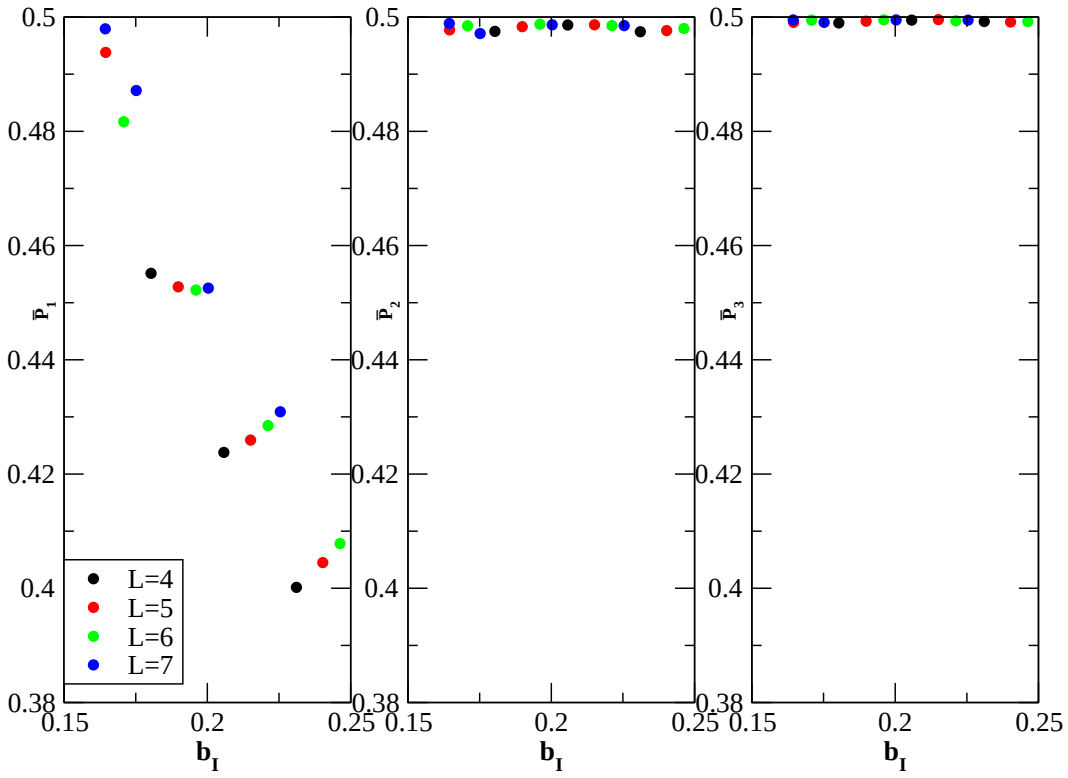

Figure 2: Plot of $\bar{P}_i$ as a function of b for all the data sets in Table 1 with $N = 59$ showing that we are in the deconfined phase.

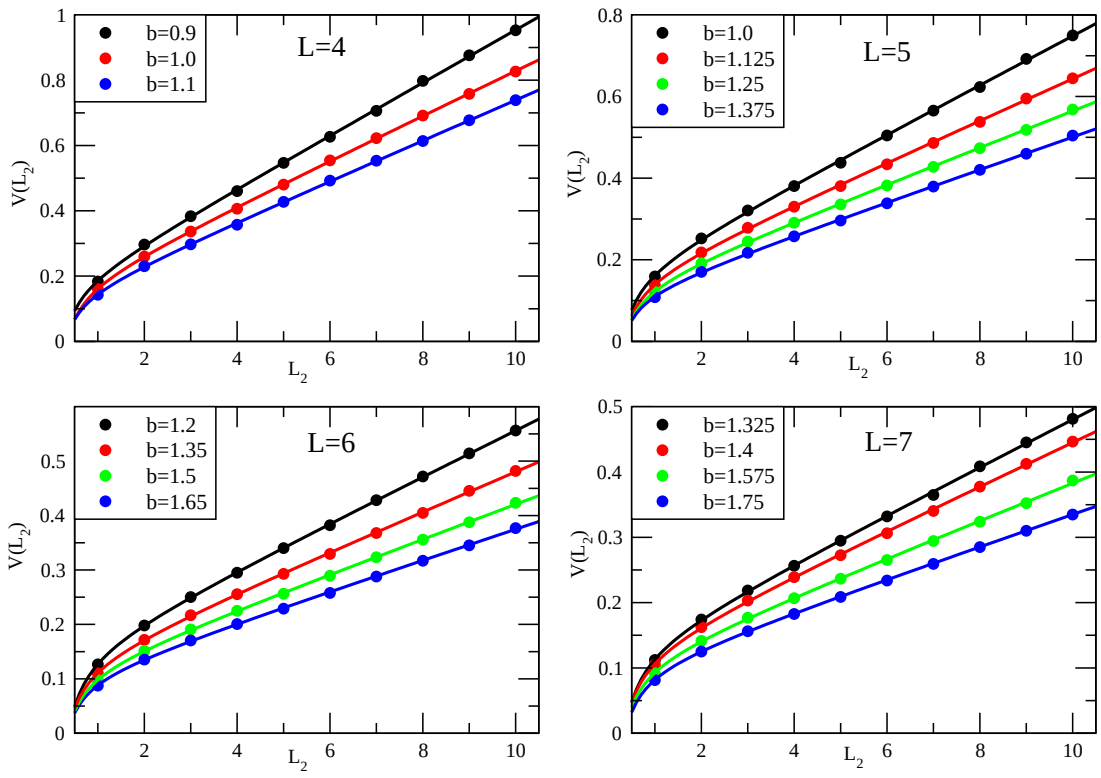

Figure 3: Plot of the static potential as a function of the separation for all the data sets in Table 1 with $N = 59$.

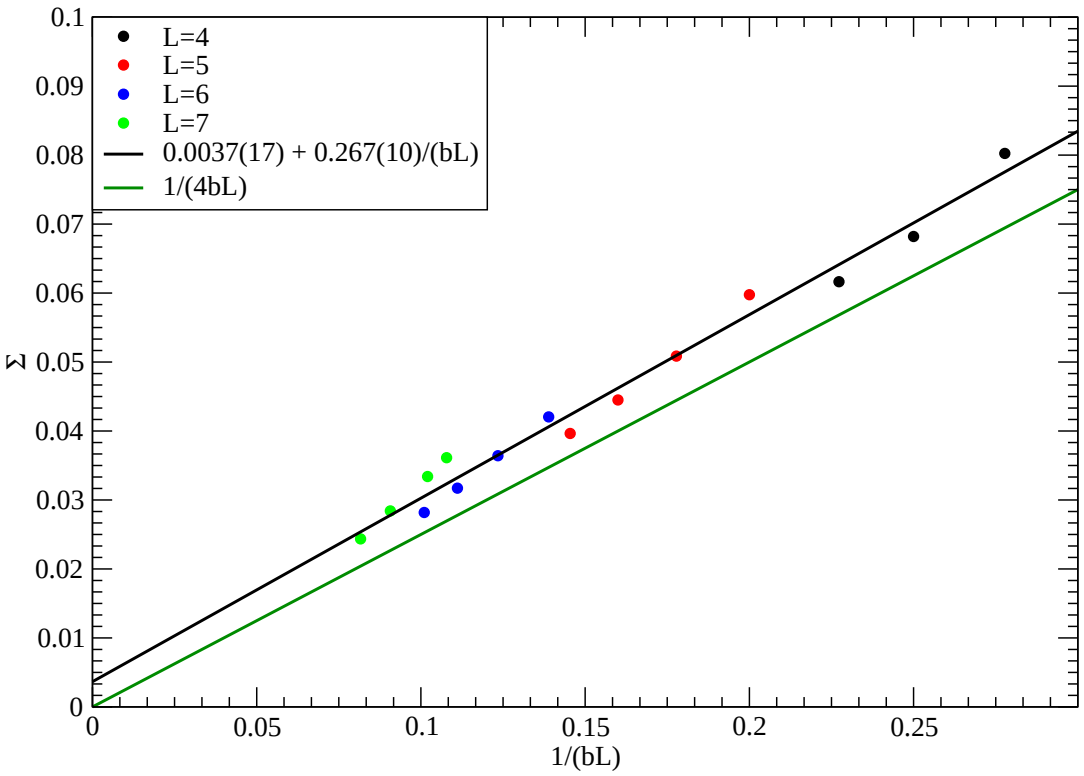

Figure 4: The spatial string tension as a function of the effective two dimensional coupling, $\frac{1}{bL}$ in the deconfined phase.

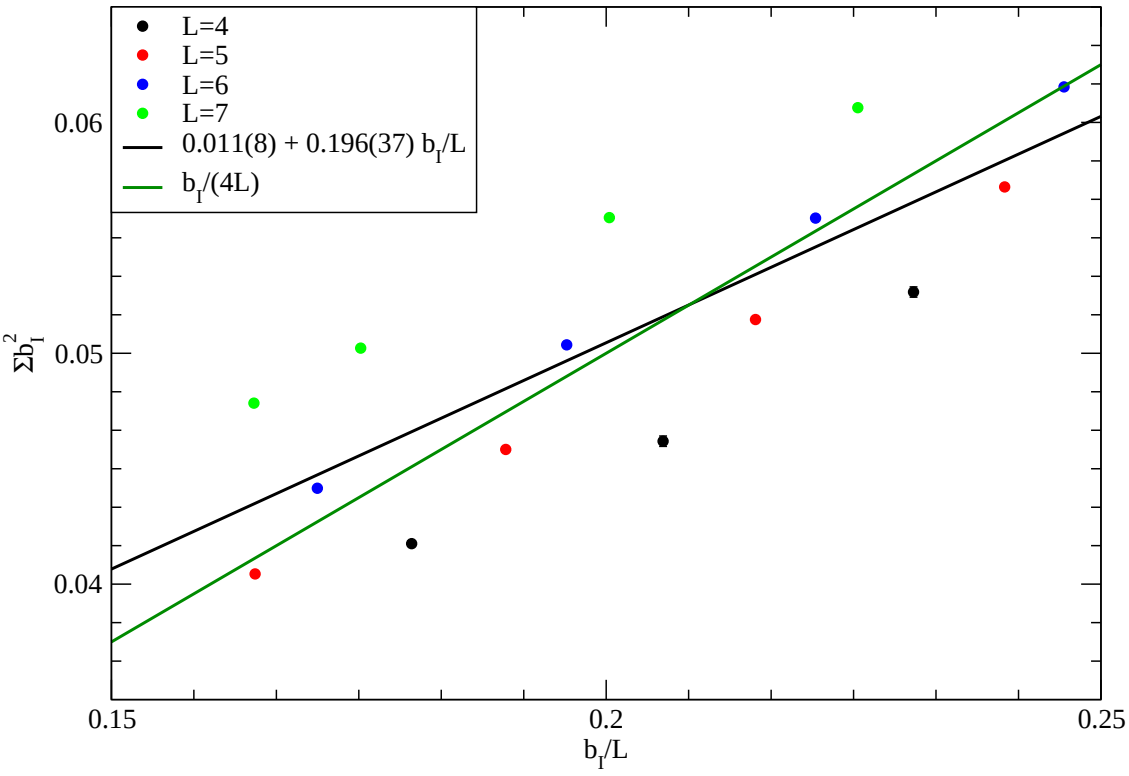

Figure 5: The dependence of the spatial string tension on the temperature in the deconfined phase.